Proceedings of the ASME 2012 Conference on Smart Materials, Adaptive Structures and Intelligent Systems
SMASIS2012
September 19-21, 2012, Stone Mountain, Georgia, USA

SMASIS2012-8253

PERFORMANCE MODELING OF A SMART MATERIAL HYDRAULIC ACTUATOR

John P. Larson
Smart Materials and Structures Laboratory
Dept. of Mechanical and Aerospace Engineering
The Ohio State University
Columbus, Ohio 43210
Email: larson.303@osu.edu

Marcelo J. Dapino *
Smart Materials and Structures Laboratory
Dept. of Mechanical and Aerospace Engineering
The Ohio State University
Columbus, Ohio 43210
Email: dapino.1@osu.edu

ABSTRACT

Smart Material Hydraulic Actuators (SMEHAs) allow high-energy-density materials, such as piezoelectrics and magnetostrictives, to be used to develop compact, high-power actuators. Hydraulic rectification using check valves converts the high-frequency, small-displacement motion of a smart material to large displacements of a hydraulic actuator. In this paper, the performance of a magnetostrictive actuator is evaluated over a range of input frequencies and loading conditions and compared to model results of the overall system. The system's dynamic performance is found to depend highly on the response of both the check valves used to rectify the motion of the smart material driver and the fluid system, including the passages connecting the smart material pump to the output hydraulic cylinder. Using AMESim, a model is developed for the response of the system and compared to experimental results.

NOMENCLATURE

α Piezomagnetic coupling coefficient
β Effective fluid bulk modulus
μ Fluid absolute viscosity
ρ Fluid density
A Area
b Damping factor
C_d, n Orifice flow coefficients
C Fluid compliance
d, l Fluid passage diameter and length
k Stiffness
F Applied force
L Fluid inertia
m Mass
P Pressure
Q Volumetric flow rate
R Flow resistance

Subscripts

acc Accumulator
A-H Fluid passages in hydraulic manifold
ch Pumping chamber
out Output hydraulic cylinder
f Friction force
ext External load force
hs High-pressure side of the output hydraulic cylinder
ls Low-pressure side of the output hydraulic cylinder
p Pumping piston

INTRODUCTION

High energy density smart materials such as magnetostrictives and piezoelectrics are potentially useful for developing compact, lightweight actuators. However, these materials produce small displacements. Electro-hydraulic actuators use hydraulic rectification to overcome this limitation; the smart material drives a pumping piston and check valves transform the

*Address all correspondence to this author.

high-force, high-frequency oscillations into large output motions of a hydraulic cylinder.

One way to increase the performance of a smart material electro-hydraulic actuators (SMEHAs) is to increase the frequency of oscillation of the pumping piston. This should increase the amount of high-pressure fluid supplied to the output hydraulic cylinder, creating higher power output. Many smart material drivers can operate in the kilohertz range, as demonstrated by Bridger et. al. [1], but for typical actuator systems the performance decreases above a few hundred hertz (Table 1). This effect is due to fluid losses (inertia and resistance) and the dynamic response of the check valves.

A significant effort has been made to improve the frequency response of the check valves used for SMEHAs. Early systems used either commercially available ball-spring valves or custom disc-spring valves, which limited their peak performance to below 100 Hz [9–11]. More recent designs use check valves that consist of a thin metal reed covering an inlet port [2, 4–6, 8]. These single reed-type valves enabled increased performance up to several hundred hertz. In order to expand the performance into the kilohertz range, miniature check valves have been developed [12–15]. Smaller valves are designed with less mass to increase the frequency response, with multiple valves arranged in an array to decrease flow resistance losses. While miniature reeds have been shown to successfully rectify fluid flow, their impact on the overall performance of the system was limited due to the limited bandwidth of the fluid system, which includes the pumping chamber, output cylinder, and connecting passages [15].

This paper presents a model that was developed to analyze the effect of the fluid system on the overall performance of the a smart material hydraulic actuator. Model equations for the individual components that make up the system, including the smart material driver, reed valves, and fluid system, are expressed and AMESim is used to calculate the system performance. The model results are validated with experimental measurements of the performance of a SMEHA system. The validated model can then be used to identify the key factors limiting the system performance.

MODEL DEVELOPMENT

Reed Valve Model

Previous studies by the authors have characterized the reed valves by comparing 3-D finite-element models with experimental measurements of the steady-state flow and corresponding pressure differential across the valves [16]. For a system model, it is desirable to express the performance of the valves in a form suitable for efficient computation. The opening area of the reeds is relatively small; therefore, the pressure differential ΔP for a given flow Q can be expressed by the orifice flow equation

$$\Delta P = \frac{\rho}{2}\frac{1}{(C_\mathrm{d}A)^n}Q^n \tag{1}$$

with the coefficients set to the typical values for a sharp-edged orifice: $n = 2$, $C_\mathrm{d} = 0.61$ (Figure 1). Since the pump is operated

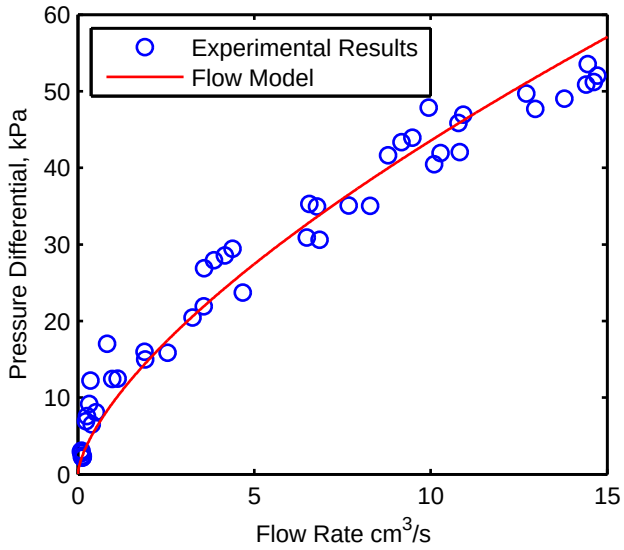

FIGURE 1. Orifice flow model of the flow over the reed valves (1) compared to measured steady-state flow vs. pressure.

at a frequency below the first natural frequency of the reed valve, the flow area A is calculated assuming that the deflection of the reed corresponds to the first bending mode of a cantilever beam (Figure 2). This results in an area of 8.5 mm^2 for every mm of tip displacement [17].

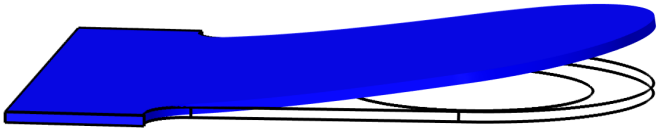

FIGURE 2. First bending mode of the reed valve, calculated using COMSOL.

The opening of the reed valve is determined by the stiffness, which was calculated using a finite element model based on the

TABLE 1. Performance comparison of smart material electro-hydraulic actuators.

Blocked Pressure [kPa]	No-Load Flowrate [cm^3/s]	Power Output (W)	Input Frequency [Hz]	Author	Year
4500*	17*	18.4	225	Larson and Dapino [2]	2012
490*	43*	5.2**	400	Chaudhuri and Wereley [3]	2010
550	19	2.6	200	Kim and Wang [4]	2010
610*	25.6*	2.5	400	John et al. [5]	2007
7600	4.6*	8.7**	165	Rupinsky and Dapino [6]	2006
21000	—	—	2400	Bridger et al. [1]	2004
8300	3.4	7.1**	1000	Lee et al. [7]	2004
1600*	3*	1.2**	300	Sirohi and Chopra [8]	2003
4000	4.2	4.2**	80	Oates and Lynch [9]	2001
4300*	4.6*	4.9**	60	Mauck and Lynch [10]	2000
34	30	0.3**	35	Gerver et al. [11]	1998

*Value calculated based on the reported blocked-force or no-load velocity values and the output cylinder area. **Estimate of power output based on the no-load flow rate and blocked pressure.

reed geometry as 2.3 kN/m (Figure 2). This value is equal to the stiffness of a rectangular cantilever beam of similar size to the reed (5 mm x 6 mm x 0.127mm). The fluid resistance model for the valves does not take into account the dynamic response (inertia) of the reed. The valve is assumed to respond instantaneously to the fluid flow, which is a reasonable approximation since the natural frequency of the reed is significantly higher than the fluid oscillation frequency.

A key factor in calculating how much the reed valve opens is determining the amount area upon which a pressure differential acts. The area was calculated from a linear fit of the static-testing results for the reed, although similar results were determined from a finite-element model of the flow over the reeds [16]. The pressure acts on an area slightly larger than the inlet area but smaller than the size of the reed tip (Figure 3).

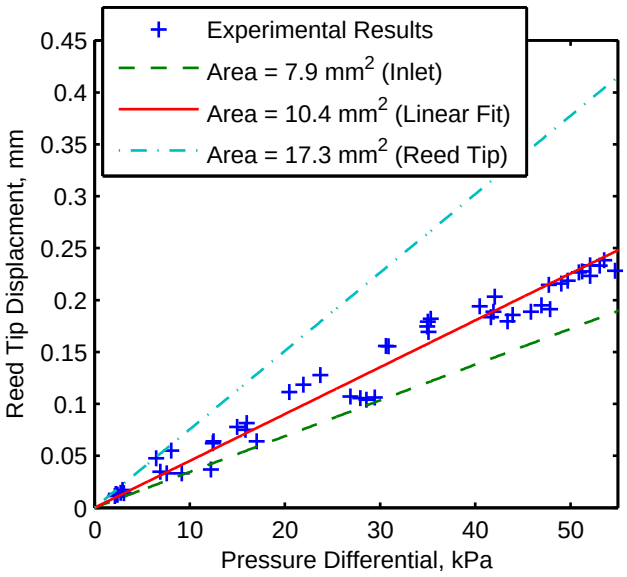

FIGURE 3. The tip displacement of the reed valve is determined by its stiffness and the amount of area that the fluid pressure is applied, is bounded by the size of the inlet and the size of reed itself.

Mechanical Sub-system

The response of Terfenol-D depends on many factors including the amount of preload, the temperature, and the operating frequency. This makes the general response nonlinear; however, a linear model is found to be sufficient for modeling the SMEHA system. The forces acting on the pumping piston include the stiffness and damping of the Terfenol-D driver, k_p and b_p, and the pressure of the fluid in the pumping chamber, P_{ch} (Figure 4). A magnetostrictive coupling coefficient, α relates the force response of the Terfenol-D driver to the applied current I [6]. The piston position x_{p} is given by

$$m_{\text{p}}\ddot{x}_{\text{p}} + b_{\text{p}}\dot{x}_{\text{p}} + k_{\text{p}}x_{\text{p}} = \alpha I - A_{\text{ch}}P_{\text{ch}} \tag{2}$$

where m_{p} represents the effective mass of the piston, metal sealing diaphragm, and Terfenol-D driver.

Similarly, the output hydraulic cylinder position x_{out}, is given by

$$m_{\text{out}}\ddot{x}_{\text{out}} + b_{\text{out}}\dot{x}_{\text{out}} + k_{\text{out}}x_{\text{out}} = A_{\text{out}}\left(P_{\text{hs}} - P_{\text{ls}}\right) - F_{\text{f}} - F_{\text{ext}} \tag{3}$$

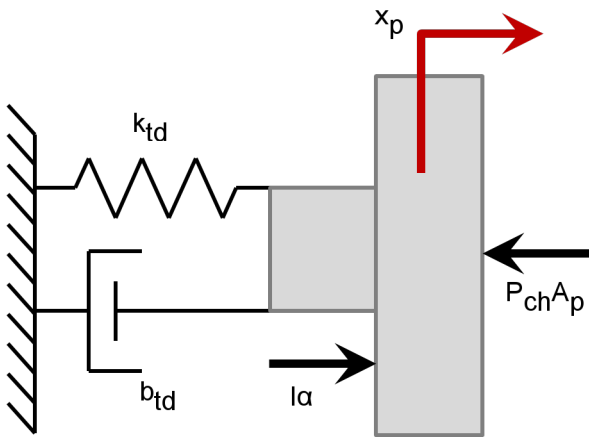

FIGURE 4. Mechanical model of the pumping piston.

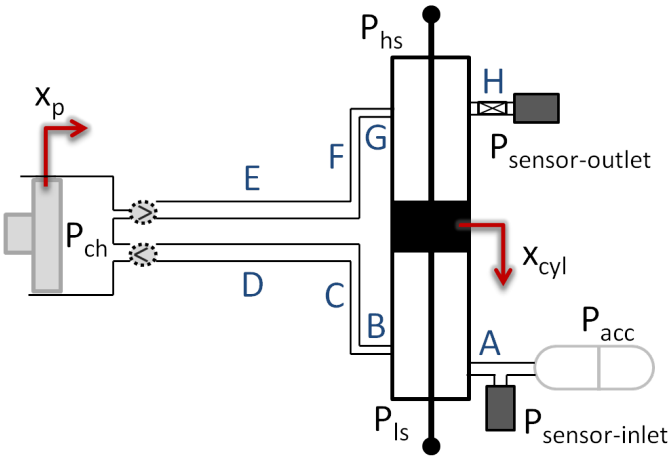

FIGURE 5. System model diagram showing the layout of the fluid passages.

where m_{out}, k_{out}, and b_{out} are the mass, stiffness, and damping of the output hydraulic cylinder and any applied load. The pressure difference acts on the cylinder area A_{out} from the high- and low-pressure sides (P_{hs} and P_{ls}). The force from external loading F_{ext}, due to applied weights in this case, and friction F_f are also considered.

Fluid Sub-system

The layout of the fluid passages within the system is shown in Figure 5. The fluid system is modeled using a lumped-parameter approach; each section of fluid passage (labeled A-H) is represented by one or more nodes which represent the passage with an equivalent resistance R, inertia L, and compliance C, given by

$$R = \frac{128\mu l}{\pi d^4},\ L = \frac{2\rho l}{d},\ \text{and}\ C = \frac{dl}{2\beta} \tag{4}$$

for a length l of fluid passage with diameter d. This results in two differential equations for the pressure P and flow Q at each node (Figure 6),

$$Q_1 - Q_2 = C\frac{dP_1}{dt} \tag{5}$$

$$P_1 - P_2 = RQ_2 + L\frac{dQ_1}{dt} \tag{6}$$

The larger volumes of fluid in the system, including the pumping chamber P_{ch}, high-pressure side of the output cylinder P_{hs}, and low-pressure side of the pumping chamber P_{ls}, are modeled using the fluid compliance given by the bulk modulus β and

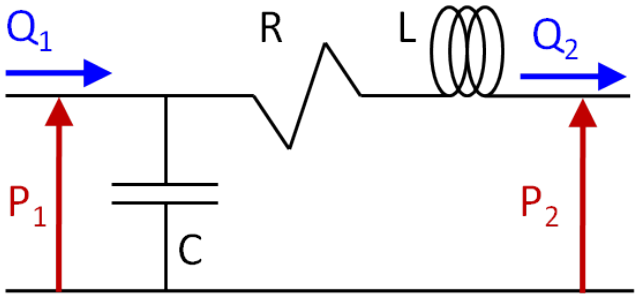

FIGURE 6. Each section of the fluid passages is modeled using one or more lumped-parameter nodes incorporating the equivalent resistance, inertia, and compliance of the fluid in the section as defined by (4).

flow in and out of each volume:

$$\left(\frac{V_{ch}}{\beta}\right)\dot{P}_{ch} = A_p\dot{x}_p - Q_{out} + Q_{in} \tag{7}$$

$$\left(\frac{V_{hs}}{\beta}\right)\dot{P}_{hs} = Q_G - Q_H - A_{out}\dot{x}_{out} \tag{8}$$

$$\left(\frac{V_{ls}}{\beta}\right)\dot{P}_{ls} = Q_A - Q_B + A_{out}\dot{x}_{out} \tag{9}$$

AMESim Implementation

The system model is implemented using the 1D, multi-domain simulation software AMESim. Figure 7 shows the circuit diagram for the complete model, which includes the mechanical components (green) of the smart material driver and output cylinder mass, hydraulic components of the pumping piston output hydraulic cylinder (red), and hydraulic lines (blue). Table 2

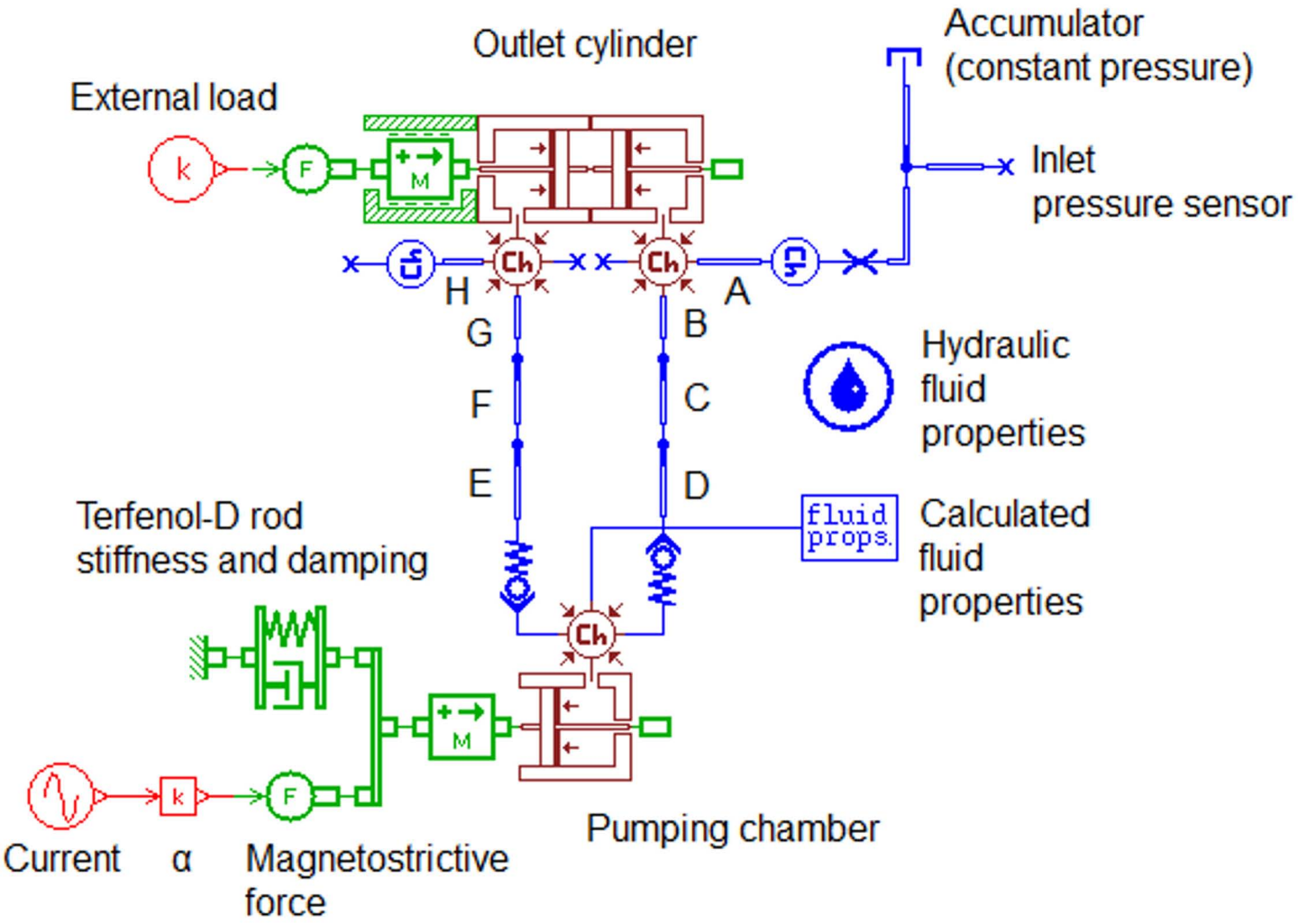

FIGURE 7. AMESim implementation of SMEHA system.

summarizes the dimensions of the fluid hydraulic lines of the system. The parameters of the Terfenol-D driver and output hydraulic cylinder are summarized in Table 3. The bulk modulus of the fluid depends highly on the amount percentage of entrained air, which is assumed to be 0.5%. Friction is modeled using a static friction force of 110 N(25 lb) and a dynamic friction force of 2.2 N (0.5 lb), which are based on measurements of the force required to manually displace the output cylinder.

PERFORMANCE TESTING

The performance of a smart material actuator was evaluated over a range of input frequencies from 100-1600 Hz. The actuator is driven by a 114-mm-long, 13-mm-diameter Terfenol-D rod. A constant sinusoidal current of 3.5 A_{RMS} was applied at all frequencies, with a bias DC current to prevent frequency doubling of the magnetostrictive driver. A bias pressure of 2.59 MPa (375 psi) was applied with a nitrogen-charged accumulator to preload the Terfenol-D driver, which prevents damage to the relatively brittle rod by keeping it in compression and improves the performance by favorably aligning the magnetic domains. In addition, the bias pressure prevents cavitation. Mobil DTE-24 hydraulic fluid was used for testing; the density of the fluid is 871 kg/m^3 and the kinematic viscosity is 80 cSt at room temperature.

Figure 8 shows the setup of the actuator used for testing. A National Instruments cDAQ-9178 system was used to record the test data and generate the drive signal, which was amplified using an AE Techron LVC 5050 linear amplifier. The output cylinder position was recorded using a string potentiometer, and a strain gage was used to measure the Terfenol-D strain. Two Sensotec TJE-5000 psi pressure sensors were provided to mea-

TABLE 2. Fluid passage dimensions for the smart material electro-hydraulic actuator.

Fluid Passage	Diameter (cm)	Length (cm)
A	0.24	0.70
B	0.24	0.87
C	0.16	2.76
D	0.32	5.72
E	0.44	5.72
F	0.16	2.76
G	0.24	0.87
H	0.24	0.95
Low-side Sensor Passage	0.70	4.57
Inlet from Accumulator	0.95	11.43

TABLE 3. Magnetostrictive driver, piston, and output hydraulic cylinder properties.

Parameter	Value	Units	Description
E_{TD}	20	GPa	Terfenol-D modulus
α	130	N/A	Coupling coefficient
m_p	124	g	Piston effective mass
k_p	24.3	MN/m	Piston effective stiffness
b_p	2.5	kN s/m	Piston effective damping
A_{ch}	0.95	cm^2	Pumping chamber area
h_{ch}	5.07	mm	Pumping chamber height
A_{out}	1.27	cm^2	Output cylinder area

sure the pressure on the both the high and low pressure sides of the output hydraulic cylinder. However, previous testing found that the extra volume associated with the high-pressure side sensor decreased the performance of the system, so the performance was evaluated using the output cylinder velocity only with the sensor volume closed off by a needle valve (at section H, Figure 5) [2].

MODEL VALIDATION

The experimental results show two peaks in the response over the frequency range (Figure 9), which is typical of SMEHA systems. The AMESim model results match this overall trend of the response, including the peaks at 275 Hz and 900 Hz.

The flow rates at frequencies of 500 Hz and above are over-predicted by the model. This is likely due to the simplified linear Terfenol-D model used in the system. Effects such as the change in Terfenol-D modulus with frequency and eddy current

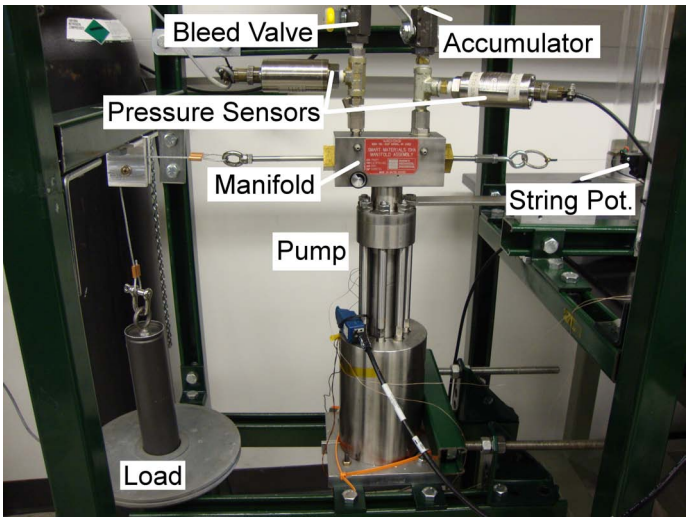

FIGURE 8. Experimental setup for smart material electro-hydraulic actuator performance evaluation.

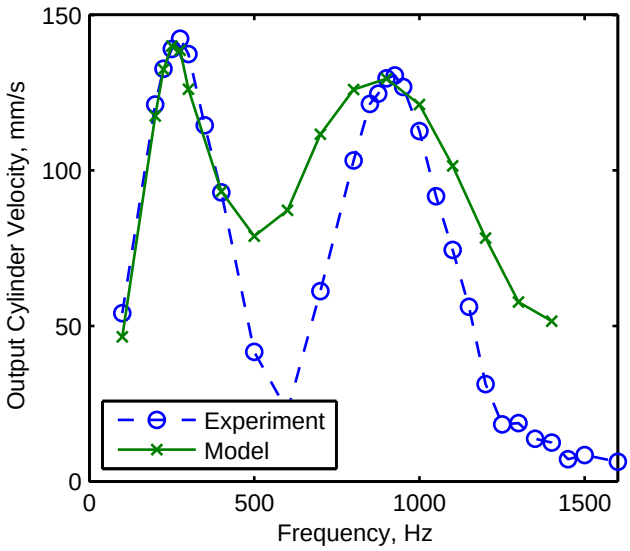

FIGURE 9. Comparison of unloaded velocity between model and experimental data.

losses are not taken into account in the model; these decrease the performance of the experimental system, especially at higher frequencies. Valve dynamics also would be expected to play an increasing role as the pumping frequency increases, which also reduce the performance of the system due to any phase lag or reverse flow allowed by the valves.

CONCLUDING REMARKS

A model for the performance of a smart material hydraulic pump was developed which includes an experimentally-verified model of the one-way reed valves. The model results show that the design of the fluid system is critical for determining the overall bandwidth of operation of the system, as the frequencies where the peak responses occur are identified using a simplified linear Terfenol-D model and neglecting the reed valve dynamic response. The model is implemented in a form that allows for optimization of the fluid system to improve the performance of future designs by increasing the frequency bandwidth of operation of the system.

ACKNOWLEDGMENT

Financial support for this research was provided by the member organizations of the Smart Vehicle Concepts Center, a National Science Foundation Industry/University Cooperative Research Center (www.SmartVehicleCenter.org), and by The Ohio State University through a Smart Vehicle Concepts Graduate Fellowship. Technical advice was provided by Tom Greetham and Tom Walters of Moog, Inc. in East Aurora, NY.

REFERENCES

[1] Bridger, K., Sewell, J., Cooke, A., Lutian, J., Kohlhafer, D., Small, G., and Kuhn, P., 2004. "High-Pressure Magnetostrictive Pump Development: A Comparison of Prototype and Modeled Performance," *Proc. SPIE,* ***5388***, p. 246.

[2] Larson, J. P., and Dapino, M. J., 2012. "Design of a Smart Material Electro-hydraulic Actuator with Improved Frequency Bandwidth," *Proc. SPIE,* ***83430K***, March.

[3] Chaudhuri, A., and Wereley, N. M., 2010. "Experimental Validation of a Hybrid Electrostrictive Hydraulic Actuator Analysis," *J. Vib. Acoust.,* ***132***(2), p. 021006.

[4] Kim, G., and Wang, K., 2010. "Enhanced Control Performance of a Piezoelectric–Hydraulic Pump Actuator for Automotive Transmission Shift Control," *Proc. Inst. Mech. Eng. D J. Automob. Eng.,* ***224***(2), pp. 161–174.

[5] John, S., Sirohi, J., Wang, G., and Wereley, N., 2007. "Comparison of Piezoelectric, Magnetostrictive, and Electrostrictive Hybrid Hydraulic Actuators," *J. Intell. Mater. Syst. Struct.,* ***18***(10), p. 1035.

[6] Rupinsky, M. J., and Dapino, M. J., 2006. "Smart Material Electrohydrostatic Actuator for Intelligent Transportation Systems," *ASME Conf. Proc.,* ***2006***(47683), pp. 721–730.

[7] Lee, D., Or, S., and Carman, G., 2004. "Design of a Piezoelectric-hydraulic Pump with Active Valves," *J. Intell. Mater. Syst. Struct.,* ***15***(2), p. 107.

[8] Sirohi, J., and Chopra, I., 2003. "Design and Development of a High Pumping Frequency Piezoelectric-Hydraulic Hybrid Actuator," *J. Intell. Mater. Syst. Struct.,* ***14***(3), pp. 135–147.

[9] Oates, W. S., and Lynch, C. S., 2001. "Piezoelectric Hydraulic Pump System Dynamic Model," *J. Intell. Mater. Syst. Struct.,* ***12***(11), pp. 737–744.

[10] Mauck, L., and Lynch, C., 2000. "Piezoelectric Hydraulic Pump Development," *J. Intell. Mater. Syst. Struct.,* ***11***(10), p. 758.

[11] Gerver, M., Goldie, J., Swenbeck, J., Shea, R., Jones, P., Ilmonen, R., Dozor, D., Armstrong, S., Roderick, R., Nimblett, F., et al., 1998. "Magnetostrictive Water Pump," *Proc. SPIE,* ***3329***, March, pp. 694–705.

[12] Li, B., and Chen, Q., 2005. "Design and Fabrication of in situ UV-LIGA Assembled Robust Nickel Micro Check Valves for Compact Hydraulic Actuators," *J. Micromech. Microeng.,* ***15***(10), p. 1864.

[13] Li, B., and Chen, Q., 2006. "Solid Micromechanical Valves Fabricated with in situ UV-LIGA Assembled Nickel," *Sensor Actuat. A-Phys.,* ***126***(1), pp. 187–193.

[14] Lee, D., Shin, D., and Carman, G., 2007. "Large Flow Rate/High Frequency Microvalve Array for High Performance Actuators," *Sensor Actuat. A-Phys.,* ***134***(1), February, pp. 257–263.

[15] Larson, J. P., and Dapino, M. J., 2012. "Reliable, High-Frequency Miniature Valves for Smart Material Electro-Hydraulic Actuators," *J. Intell. Mater. Syst. Struct.,* ***23***(7), March, pp. 801–809.

[16] Larson, J., and Dapino, M., 2011. "High-frequency Valve Development for Smart Material Electro-hydraulic Actuators," *Proc. SPIE,* ***7979***, p. 79790E.

[17] Blevins, R. D., 1979. *Formulas for Natural Frequency and Mode Shape*. Van Nostrand Reinhold Company.